

# Coupled Thermal Conductivity Dryout Curve and Soil–Water Characteristic Curve in Modeling of Shallow Horizontal Geothermal Ground Loops

Ray Wu · James M. Tinjum · William J. Likos

Received: 7 December 2013 / Accepted: 21 August 2014 / Published online: 3 September 2014  
© Springer International Publishing Switzerland 2014

**Abstract** Shallow horizontal ground loops harness stored subsurface thermal energy and operate in conditions where the moisture and temperature of the surrounding soil vary spatially and temporally. The thermal conductivity of the soil is dependent on soil moisture and temperature and is a design parameter that greatly influences the size and performance of horizontal ground loops. However, soil thermal conductivity is often assumed to be constant and conservative estimates are used in the design of ground loops. Two fundamental constitutive relationships, the thermal conductivity dryout curve (TCDC) and the soil–water characteristic curve (SWCC), can be coupled and used to quantify transient moisture-dependent thermal behavior of soil. In this study, coupled TCDCs and SWCCs were utilized in two-dimensional models based on the finite-element method to predict moisture migration effects on transient hydraulic and

thermal behavior of unsaturated soil surrounding geothermal exchange loops. Soil thermal conductivity predicted from using coupled TCDCs and SWCCs are compared to the conventional method of using a conservative value. Results suggest that employing coupled TCDCs and SWCCs can provide realistic and improved values of soil thermal conductivity for the design of horizontal ground loops.

**Keywords** Horizontal ground loop · Thermal conductivity dryout curve · Soil–water characteristic curve · Soil thermal conductivity · Coupled heat and moisture flow · Geothermal heat exchanger

## 1 Introduction

Ground-source heat pump (GSHP) systems utilize buried ground loops (i.e., geothermal heat exchangers) to transfer heat between the ground and a heat pump for heating and cooling of a building. The subsurface is generally an effective thermal source and sink because ground temperatures become relatively stable with increasing depth below ground surface (bgs) and nearly constant at 5 m bgs year round (Kusuda and Achenbach 1965; Williams and Gold 1976; Florides and Kalogirou 2007). In comparison to traditional heating, ventilation, and air conditioning (HVAC) systems, GSHP systems offer benefits of reduced greenhouse gas emissions, high reliability, low

---

R. Wu (✉)  
Geosyntec Consultants, Kennesaw, GA 30144, USA  
e-mail: rwu@geosyntec.com

J. M. Tinjum  
Department of Engineering Professional Development,  
University of Wisconsin-Madison, Madison, WI 53706,  
USA  
e-mail: jmtinjum@wisc.edu

W. J. Likos  
Department of Geological Engineering, University of  
Wisconsin-Madison, Madison, WI 53706, USA  
e-mail: likos@wisc.edu

maintenance, and lower energy, operating, and life-cycle costs (Inalli and Esen 2005; Tarnawski et al. 2009; Congedo et al. 2012). Despite these advantages, however, the design of the ground loop may be highly conservative, which then may lead to high initial capital costs that continue to hinder consumer appeal and implementation.

For smaller heat load applications, such as residential and commercial heating and cooling, shallow vertical or horizontal ground loops are used. When a sufficient footprint is available, shallow horizontal ground loops are cost effective because trench installation equipment is widely available and inexpensive compared to borehole drilling. In horizontal configurations, the ground loop is typically buried 1–2 m bgs and a fluid (e.g., water) is circulated within the loop, transferring heat from the ground to the ground loop or vice versa. The second law of thermodynamics places constraints upon the direction of heat transfer to and from the ground loop. For example, in the winter, the ground loop extracts heat (i.e., heating mode) from the ground since the ground temperature is warmer than the air temperature. Conversely, in the summer, the ground loop rejects heat (i.e., cooling mode) to the ground since the ground temperature is cooler than the air temperature.

The design of a horizontal ground loop is complex and depends on numerous parameters that include the arrangement of the horizontal trenches, specifications of the heat pump (i.e., capacity, flow rate, electrical demand, and efficiency), thermal properties of the soil and heat exchanger pipe, fluid flow rate in the ground loop, ground temperature, and geographic climate. Within the past decade, a number of parametric studies using numerical modeling analyses have been conducted to predict the performance of horizontal ground loops. Demir et al. (2009) developed a numerical model to investigate surface climate effects on heat transfer through parallel horizontal pipes. Wu et al. (2010) used computational fluid dynamics (CFD) software to predict the thermal performance of horizontal slinky ground loops and discussed the effects of coil diameter and interval distance. Benazza et al. (2011) performed quasi three-dimensional numerical simulations of horizontal ground loops to investigate the effects of operation conditions, loop spacing, loop diameter, and soil thermal conductivity ( $\lambda_{\text{soil}}$ ). Congedo et al. (2012) also used CFD software to evaluate the effect of geometrical (e.g., loop diameter, pitch,

and depth) and functional (e.g., fluid flow rate in loop and  $\lambda_{\text{soil}}$ ) parameters on straight, helical, and slinky horizontal ground loops. Additionally, Chong et al. (2012) used CFD software to evaluate the effects of loop diameter, loop pitch, and thermal properties of soil on the thermal performance of horizontal slinky heat exchangers. A common finding among these studies was that the  $\lambda_{\text{soil}}$  surrounding the ground loop had a significant effect on the thermal performance of horizontal ground loops. Congedo et al. (2012) concluded that  $\lambda_{\text{soil}}$  was the most important parameter for heat transfer performance of the GSHP system. However, a shared limitation in these studies was that constant and uniform values of  $\lambda_{\text{soil}}$  were assumed for their simulations.

Soil thermal conductivity governs the rate of conductive heat flow through soil and is defined as the quantity of heat transfer through a unit area of soil in a unit of time under a unit temperature gradient. Using a constant value of  $\lambda_{\text{soil}}$  in transient conditions is imprudent because  $\lambda_{\text{soil}}$  can vary with soil composition, soil density, soil moisture content, and temperature (Farouki 1981; Salomone and Kovacs 1984; Woodward et al. 2013). For horizontal ground loops, variability of  $\lambda_{\text{soil}}$  is primarily expected as a result of changing moisture conditions. Generally, horizontal ground loops are installed in a single type of backfill and a certain soil density can be achieved through compaction. During operation of the ground loop, the density of the backfill does not change significantly. Varying temperatures of the backfill are expected from operation of the ground loop as well as seasonal fluctuations. However, the range of temperatures around an operating ground loop is only a few degrees (Demir et al. 2009; Wu et al. 2010). Changes in  $\lambda_{\text{soil}}$  as a function of temperature generally occur over wider temperature ranges (Smits et al. 2012). Spatial and temporal variations of soil moisture content are not as easily predicted due to the complex cycle of moisture migration mechanisms, including thermally induced moisture migration, groundwater table (GWT) fluctuations, and climatic variations. Therefore, a variable value of  $\lambda_{\text{soil}}$  as a function of soil moisture would better characterize unsaturated soil conditions in horizontal ground loop modeling.

The thermal conductivity dryout curve (TCDC) for a soil defines the relationship between moisture content (gravimetric water content, volumetric water content, or degree of saturation) and thermal conductivity ( $\lambda$ ),

and thus quantifies the moisture-dependent thermal behavior of soil. The retention of water in unsaturated soil can be predicted from the soil–water characteristic curve (SWCC), which defines the relationship between moisture content and suction ( $\psi$ ). Furthermore, to predict the rate of water movement, the SWCC can be used to estimate the hydraulic conductivity curve, which defines the relationship between moisture content and hydraulic conductivity ( $k$ ). The TCDC and SWCC are characteristic functions for a given soil, and when coupled, govern the transport of heat and moisture. With various model estimation and experimental techniques available (e.g., Côté and Konrad 2005; Likos et al. 2012; Woodward et al. 2013; Fredlund and Xing 1994; Agus and Schanz 2005) as well as a growing base of literature with published values (e.g., Campbell et al. 1994; Leij et al. 1996; Smits et al. 2010; Krishnapillai and Ravichandran 2012), TCDCs and SWCCs are now relatively easy to obtain and are useful for modeling coupled heat and moisture flow.

In this study, coupled TCDCs and SWCCs were integrated in the modeling of coupled heat and moisture transfer present in unsaturated soil surrounding a shallow horizontal ground loop. Specifically, the significance of moisture migration on predicting values of in situ  $\lambda_{\text{soil}}$  was evaluated. Values of  $\lambda_{\text{soil}}$  predicted from backfill with experimentally measured TCDCs and SWCCs are compared with the conventional method of using conservative and constant  $\lambda_{\text{soil}}$ . Moreover, the importance of selecting a value of  $\lambda_{\text{soil}}$  is demonstrated by using simulation results to quantify changes in thermal performance and length of horizontal ground loop for a GSHP system using a heat pump with nominal 3-ton (10.55 kW) capacity and coefficient of performance (COP) of four.

## 2 Soil Properties

Three quartz-rich sands—hereby referred to as soil A, B, and C—were selected as backfill for the current simulations of horizontal ground loops. Quartz sands are favored for use as backfill due to their favorable thermal properties ( $\lambda_{\text{quartz}} = 8 \text{ W/mK} > \lambda_{\text{fines}} = 2.9 \text{ W/mK} > \lambda_{\text{water}} = 0.6 \text{ W/mK} \gg \lambda_{\text{air}} = 0.024 \text{ W/mK}$ ). Grain-size distribution (ASTM D422-63), standard Proctor compaction (ASTM D698-12), and X-ray diffraction techniques were performed to

**Table 1** Physical characteristics of selected backfill soils A, B, and C

Soil	USCS <sup>a</sup> ID	D <sub>10</sub> <sup>b</sup> (mm)	Quartz (%)	Fines (%)	$\gamma_{\text{dry,max}}^c$ (kN/m <sup>3</sup> )
A	SP	0.18	69.1	0.57	17.89
B	SP	0.13	77.4	2.0	18.55
C	SW	0.13	78.2	3.13	19.53

<sup>a</sup> USCS = unified soil classification system (ASTM D2487-11)

<sup>b</sup> D<sub>10</sub> = soil particle diameter at 10 % finer (ASTM D422-63)

<sup>c</sup>  $\gamma_{\text{dry,max}}$  = maximum dry unit weight (ASTM D698-12)

determine physical characteristics of the soils, as shown in Table 1.

The three soils were compacted to approximately 90 % maximum dry unit weight to determine TCDCs and SWCCs using the automated hanging column method outlined in Smits et al. (2010). The automated hanging column method can be used to simultaneously determine the TCDC and SWCC of coarse-grained soils through the continuous collection of data from a dielectric moisture content sensor, temperature probe, tensiometer, and dual-needle thermal probe embedded in the specimen. The TCDCs and SWCCs were obtained at room temperature (i.e., 21 °C) during a drying process as pore water was allowed to drain through specimens along an initial drainage path. The experimentally determined TCDCs and SWCCs of each soil in terms of degree of saturation ( $S$ ) are shown in Fig. 1a, b, respectively. While TCDCs at elevated temperatures (e.g., >50 °C) can display nonmonotonic behavior with a maximum at low saturation (e.g., Smits et al. 2012), the monotonically decreasing TCDCs presented in Fig. 1a were implemented in the current simulations since relatively low temperatures (e.g., less <30 °C) were used.

A key feature on both the TCDC and SWCC is the residual saturation (arrows at the knee of the curves) in Fig. 1a, b. Knowledge of the residual saturation provides an indicator for thermal instability. In the TCDC, the residual saturation, which is also referred to as the critical saturation, defines the point at which incremental decreases in saturation result in a significant decreases in thermal conductivity. Likewise, in the SWCC, the residual saturation defines the point at which incremental decreases in saturation require much greater suctions. Moisture migration due to thermal and hydraulic gradients can create dry soil

**Fig. 1** **a** TCDCs and **b** SWCCs of backfill soils A, B, and C

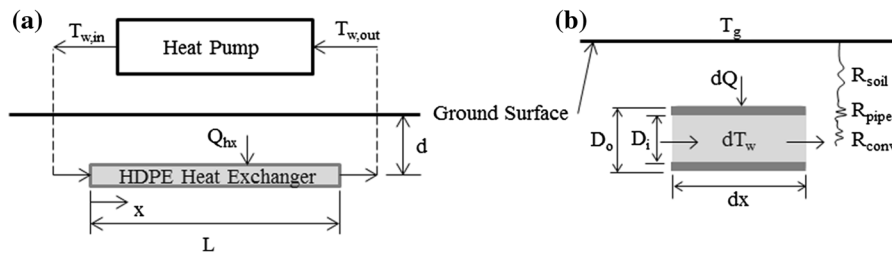
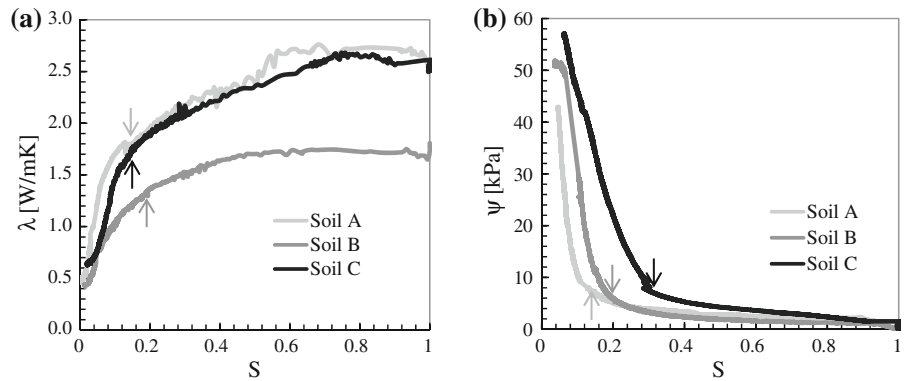


**Fig. 2** **a** Simple GSHP system schematic and **b** ground loop differential element

conditions around the ground loop and continued drying below the residual saturation results in significant reductions of  $\lambda_{soil}$ . If the developed dry zone persistently inhibits dissipation of heat from the ground loop, a thermal runaway condition may ensue. As a preventative measure, a conservative estimate of  $\lambda_{soil}$  usually corresponds to a value below the residual saturation. However, there is still a wide range of saturations ( $\sim 0.3 < S < 1.0$ ) where higher  $\lambda_{soil}$  exists.

### 3 Simplified Heat Transfer Model

Heat transfer in the ground is challenging because the ground temperature gradients vary spatially and temporally. In this study, a simplified heat transfer model was used as a more manageable approach to estimate model input parameters and to approximate the length of ground loops based on predicted values of  $\lambda_{soil}$  influenced by moisture migration mechanisms relevant to horizontal ground loops. By assuming isothermal boundary conditions at the ground loop and ground surface, a thermal resistance network involving a conduction shape factor for a horizontally buried cylinder is applicable. The thermal resistance

approach is analogous to the Neher and McGrath (1957) method used to model heat transfer mechanisms in underground cable installations for calculating cable ampacity. An approximate length of ground loop for a given heat pump capacity and COP can be derived from an energy balance on the GSHP system and differential element shown in Fig. 2. The capacity of the heat pump was assumed to represent the required building load (i.e., energy demand).

Based on known values of the heat pump capacity ( $Q_{hp}$ ), heat pump efficiency (COP or energy efficiency ratio (EER)), fluid flow rate ( $m_w$ ), and entering water temperature (EWT =  $T_{w,out}$ ), the heat exchanger load ( $Q_{hx}$ ) and leaving water temperature (LWT =  $T_{w,in}$ ) can be determined by:

$$COP = \frac{\text{power output}}{\text{power input}} = \frac{Q_{hp}}{Q_{hp} - Q_{hx}} \tag{1}$$

$$EER = \frac{\text{cooling energy output}}{\text{electrical energy input}} = \frac{Q_{hp}}{Q_{hx} - Q_{hp}} \tag{2}$$

$$Q_{hx} = m_w c_{wp} \Delta T_w \tag{3}$$

where  $c_{wp}$  is the specific heat capacity of the fluid at constant pressure and  $\Delta T_w$  is the temperature difference of the fluid ( $\Delta T_w = T_{w,out} - T_{w,in} =$

EWT – LWT). The rate of heat transferred per unit length between the heat exchanger fluid ( $T_w$ ) and ground ( $T_g$ ) can be determined by:

$$Q = \frac{(T_g - T_w)}{R_{total}} \tag{4}$$

Depending on whether the ground loop is used to extract or reject heat,  $Q$  may be positive (i.e., heating mode) or negative (i.e., cooling mode). If  $T_g$  is assumed to be the temperature at the ground surface, then the total thermal resistance ( $R_{total}$ ) for a horizontal pipe with inner diameter ( $D_i$ ) and outer diameter ( $D_o$ ) buried at a certain depth ( $d$ ) is the sum of resistances (i.e., inverse of conductivity) from fluid convection ( $R_{conv}$ ), pipe conduction ( $R_{pipe}$ ), and soil conduction ( $R_{soil}$ ):

$$R_{total} = R_{conv} + R_{pipe} + R_{soil} \tag{5}$$

$$R_{conv} = \frac{1}{h_w \pi D_i} \tag{6}$$

$$R_{pipe} = \frac{\ln\left(\frac{D_o}{D_i}\right)}{2\pi \lambda_{pipe}} \tag{7}$$

$$R_{soil} = \frac{1}{SF \lambda_{soil}} \tag{8}$$

In Eq. (6), the fluid properties necessary to determine the heat transfer coefficient ( $h_w$ ) are evaluated at the average fluid temperature ( $T_{avg}$ ) since variations with temperature are not significant (Incropera et al. 2006). The Nusselt number ( $N_u$ ) and Gnielinski correlation (Eq. 10) can be used to determine  $h_w$ :

$$T_{avg} = \frac{T_{w,in} + T_{w,out}}{2} \tag{9}$$

$$N_u = \frac{h_w D_i}{\lambda_w} = \frac{(f/8)(Re - 1000)Pr}{1 + 12.7(f/8)^{1/2}(Pr^{2/3} - 1)} \tag{10}$$

$$f = (0.79 \ln(Re) - 1.64)^{-2} \tag{11}$$

where  $\lambda_w$  is the thermal conductivity of the fluid,  $f$  is the Darcy friction factor,  $Re$  is the Reynolds number (i.e., ratio of inertial to viscous forces), and  $Pr$  is the Prandtl number (i.e., ratio of momentum to thermal diffusivity). The Gnielinski correlation is valid for  $0.5 \leq Pr \leq 2,000$  and  $3,000 \leq Re \leq 5 \times 10^6$  (Incropera et al. 2006). For the design of a horizontal ground loop, the circulating fluid flow rate and pipe diameter are chosen to maintain turbulent flow (i.e.,

$Re > 4,000$ ) to enhance heat transfer. In Eq. (7),  $\lambda_{pipe}$  is the thermal conductivity of the heat exchanger pipe which is typically made of high-density polyethylene (HDPE). In Eq. (8),  $SF$  is the conduction shape factor for a horizontally buried cylinder between two defined temperatures (Incropera et al. 2006):

$$SF = \frac{2\pi}{\ln\left[\left(\frac{2d}{D_o}\right) + \sqrt{\left(\frac{2d}{D_o}\right)^2 - 1}\right]} \tag{12}$$

An energy balance on the differential element, where  $Q_{hx} = Q$ , produces the differential heat transfer:

$$dQ = m_w c_{wp} dT_w = \frac{(T_g - T_w)}{R_{total}} dx \tag{13}$$

By separation of variables, integration, and application of boundary conditions shown in Fig. 2 ( $T = T_{w,in}$  at  $x = 0$  and  $T = T_{w,out}$  at  $x = L$ ), the length of ground loop ( $L$ ) can be estimated by:

$$L = m_w c_{wp} R_{total} \ln\left[\frac{(T_g - T_{w,in})}{(T_g - T_{w,out})}\right] \tag{14}$$

At constant  $m_w$  and defined temperatures,  $T_g$  and  $\Delta T_w$ , Eq. (14) suggests  $\lambda_{soil}$  (incorporated in  $R_{total}$ ) is a key variable that influences the length of ground loop since  $\lambda_{soil}$  can vary from coupled heat and moisture flow. However, in current state-of-practice, a conservative value of  $\lambda_{soil}$  representative of the greatest soil resistance expected during long-term operation of the ground loop is often estimated or assumed for the ground formation into which the ground loop will be installed (ASHRAE 2007; Remund and Carda 2009). While designing conservatively for the worst-case scenario may appear as prudent, oversized ground loops may be inefficient and more costly to install and operate. Since  $\lambda_{soil}$  is one of the most influential design parameters, an improved approach to simulate actual operating conditions is to predict variable values of  $\lambda_{soil}$  that characterize unsaturated soil behavior.

#### 4 Numerical Modeling of Coupled Heat and Moisture Flow

Coupled heat and moisture flow in unsaturated soil is a combination of conductive heat transfer and moisture

transfer under hydraulic and temperature gradients. Thermal energy transferred by the movement of fluids (i.e., groundwater flow) can also contribute convective heat transfer. In the current study, the SVHeat and SVFlux programs of SoilVision® Systems' SVOOffice (a finite-element software package) were used to simulate coupled heat and moisture transfer in unsaturated soils around a shallow horizontal ground loop. The SVHeat program allowed for the input of soil TCDCs (i.e., Fig. 1a). Additionally, the SVFlux program allowed for the input of soil SWCCs (i.e., Fig. 1b) and was used to fit the SWCCs with the van Genuchten (1980) equation to estimate the hydraulic conductivity curve. Finite-element modeling was utilized to solve the complex and nonlinear governing equations for coupled heat and moisture flow. In SVHeat and SVFlux, moisture flow (i.e., liquid flow, vapor flow, and freezing) is governed by Eq. (15) and heat flow is governed by Eq. (17) (Thode and Zhang 2009):

$$\frac{\partial}{\partial y} \left[ \left( \frac{k_y^w + k^{vd}}{\gamma_w} \right) \frac{\partial u_w}{\partial y} + k_y^w + \left( \frac{k^{vd}(-u_w)}{\gamma_w(274.15 + T)} \right) \frac{\partial T}{\partial y} \right] = \frac{\partial \theta_w}{\partial t} + \frac{\rho_i}{\rho_w} \frac{\partial \theta_{wi}}{\partial t} \quad (15)$$

$$k^{vd} = \gamma_w \frac{\omega_v u_v^{soil}}{\rho_w R(T + 273.15)} \frac{D^{v*}}{\rho_w} \quad (16)$$

$$\frac{\partial}{\partial y} \left[ \left( \frac{L_f k_y^w + L_v k^{vd}}{\gamma_w} \right) \frac{\partial u_w}{\partial y} + (\lambda + (L_v + L_f)) \times \left( \frac{k^{vd}(-u_w)}{\gamma_w(274.15 + T)} \right) \frac{\partial T}{\partial y} + L_f k_y^w \right] - C_w q_y^w \frac{\partial T}{\partial y} = (C + L_f m_2) \frac{\partial T}{\partial t} \quad (17)$$

where  $k_y^w$  is hydraulic conductivity;  $k^{vd}$  (Eq. 16) is water vapor conductivity by diffusion within the air phase;  $\omega_v$  is the molecular weight of water vapor;  $u_v^{soil}$  is soil–water vapor pressure;  $R$  is the universal gas constant;  $D^{v*}$  is vapor diffusivity through soil;  $T$  is temperature;  $u_w$  is pore water pressure;  $\gamma_w$  is the unit weight of water;  $\theta_w$  is volumetric water content;  $\theta_{wi}$  is volumetric ice content;  $\rho_w$  is water density;  $\rho_i$  is ice density;  $y$  is elevation;  $t$  is time;  $L_f$  is the mass latent heat of fusion of water;  $L_v$  is the volumetric latent heat of water vaporization;  $C_w$  is the volumetric heat

capacity of water;  $q_y^w$  is water flow flux;  $C$  is the volumetric heat capacity of soil; and  $m_2^i$  is the slope of the soil-freezing characteristic curve. In 2D modeling, partial derivative terms with respect to the x-axis ( $\partial/\partial x$ ) are incorporated. Equations (15) and (17) are coupled through the ice content ( $\theta_{wi}$ ) and vapor ( $k^{vd}$ ) terms.

## 5 Simulation Methodology

A two-dimensional (2D) cross-sectional modeling domain was evaluated to compare the thermal performance of a single horizontal ground loop in a two-pipe, trench configuration (Fig. 3). The 2D cross-section approach is reasonable if the cross-section is taken through the mid-section of the trench along the direction of fluid flow (Chiasson 2010). Furthermore, the 2D approach provides the benefit of reduced computational time.

The model domain was 8-m wide by 12-m deep with an initial groundwater table (GWT) located 2.5-m bgs. The size of the domain was assumed to be sufficiently large to encompass the expected thermally-disturbed area from operation of the single ground loop. Native soil was simulated as a sandy loam with thermal ( $\lambda_{soil} = 0.8$  W/mK) and hydraulic (Table 2) properties derived from Abu-Hamdeh and Reeder (2000) and Leij et al. (1996), respectively. Due to symmetry about the y-axis, symmetrical heat transfer in the ground was assumed and zero-flux boundary conditions (BC) were applied to the left and right side of the domain. The top surface boundary was defined by daily air temperature and precipitation. Approximated air temperature and precipitation data (Fig. 4a) were used to reduce computational time. The domain was assumed to be deep enough for the bottom boundary temperature to remain constant at 10 °C, which is the approximate groundwater temperature of northern continental United States. Furthermore, the bottom boundary was defined by varying total head values to simulate a fluctuating GWT (Fig. 4b). Since several databases were used to obtain climatic data, the precipitation and GWT data were not perfectly coupled. However, both precipitation and fluctuating GWT conditions were used to more accurately represent possible mechanisms for moisture migration.

For a typical horizontal two-pipe configuration, a single 1-m-wide by 2-m-deep trench was centered

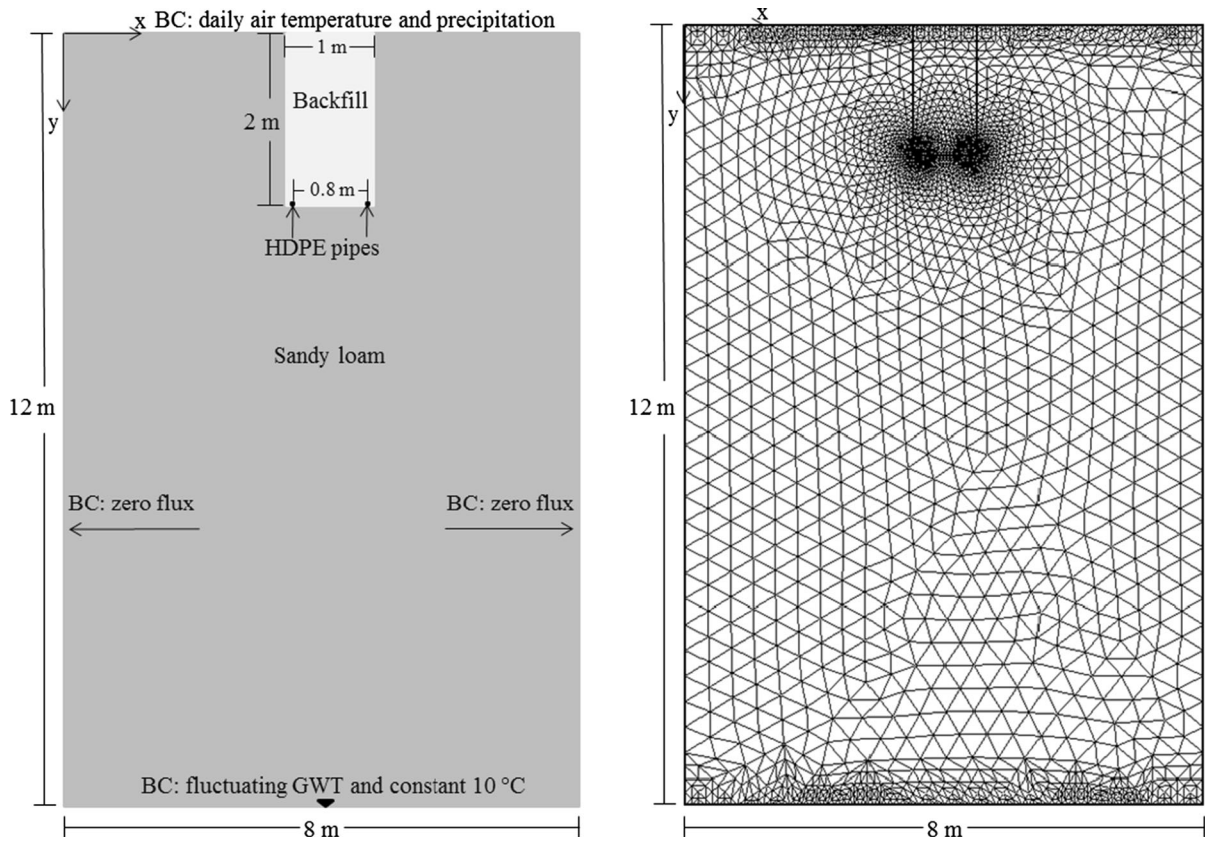


**Fig. 3** Geometry, boundary conditions (BC), and finite-element mesh

**Table 2** Hydraulic parameters of sandy loam and backfill soils

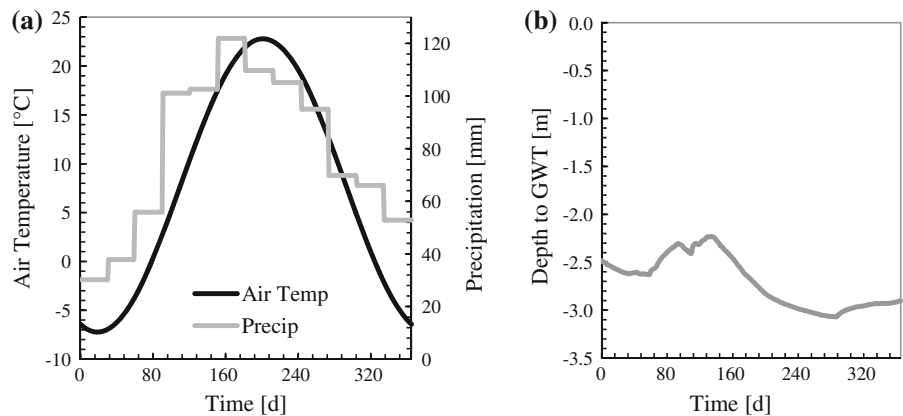
Soil	van Genuchten (1980) parameters				$k_{sat}$ (m/d)
	$\theta_{w,r}$ ( $m^3/m^3$ )	$\theta_{w,sat}$ ( $m^3/m^3$ )	$\alpha$ ( $kPa^{-1}$ )	$n$ (-)	
Sandy loam	0.13	0.37	0.21	1.61	0.6
A	0.04	0.38	0.40	3.34	28
B	0.04	0.35	0.73	2.24	13
C	0.06	0.25	0.33	2.72	15

within the model domain at the ground surface. Within the trench, two parallel SDR-11 (32-mm nominal diameter) HDPE pipes were buried 1.97-m deep and separated along the x-axis by 0.8 m. As part of the simplified heat transfer model, the HDPE pipes were modeled as constant temperature elements equivalent to the average of a design EWT suggested in ASHRAE (2007) and LWT calculated by Eq. (3). The average

fluid temperature (e.g.,  $T_{avg} = -2.84\text{ }^\circ\text{C}$  in heating and  $T_{avg} = 29.37\text{ }^\circ\text{C}$  in cooling for a heat pump with 3-ton capacity and COP of 4) was also used to specify thermophysical properties of the fluid and determine the convective heat transfer coefficient from forced convection in turbulent pipe flow (Eq. 10). The fluid was assumed to be a mixture of water and 20 % by volume propylene glycol antifreeze since design temperatures were expected to fall below the freezing point of water.

The backfill in the trench was simulated using soils A, B, and C. Two simulations were performed for each of the three backfill soils. One simulation used the soil’s experimentally measured TCDC and the other simulation used a conservative value of  $\lambda_{soil}$  selected from between the dry and residual saturation of the soil’s TCDC. For the conservative analyses, a constant value of 0.7 W/mK was selected for soils A and B since both soils had similar values of  $\lambda_{soil}$  below their residual saturation. A constant value of 0.8 W/mK was

**Fig. 4** **a** Daily air temperature and precipitation used for top BC and **b** depth to GWT below ground surface for bottom BC



selected for soil C. Each simulation was performed for 365 days beginning on the 1st of January to encompass a heating mode followed by cooling mode and returning to heating mode. The ground loop was simulated to operate in the heating mode during measured heating degree days (e.g., 253 days when the average air temperature is greater than the reference temperature,  $T_{ref} = 18.33$  °C) or cooling mode during cooling degree days (e.g., 112 days when the average air temperature is less than  $T_{ref}$ ). For each simulation, the initial ground temperature at any depth (i.e.,  $y$ ) was approximated by a pure harmonic function (Hillel 1982):

$$T_g(y, t) = T_a + A_o e^{(y/\sqrt{2\alpha/\omega})} \sin \left[ \frac{2\pi(t - t_o)}{365} - \frac{y}{\sqrt{2\alpha/\omega}} - \frac{\pi}{2} \right] \quad (18)$$

where  $T_a$  is the average ground temperature,  $A_o$  is the annual amplitude of the ground temperature,  $\alpha$  is soil thermal diffusivity,  $\omega$  is the annual angular frequency,  $t$  is time, and  $t_o$  is the time lag from an arbitrary starting date (usually January 1) to the occurrence of the minimum temperature in year. The initial hydraulic conditions were prescribed from the initial groundwater table location and corresponding partially saturated soil resulting from equilibrium capillary rise. The soil skeleton was assumed to be rigid and deformations were not considered. The SVFlux and SVHeat programs were fully coupled and performed simultaneously during simulation to determine transient moisture and temperature profiles of the ground.

## 6 Results

### 6.1 Moisture Variation

In the case of precipitation infiltration from the top of the trench and a fluctuating GWT near the bottom of the trench, soil moisture varied spatially and temporally. Figure 5a shows the volumetric water content ( $\theta_w$ ) time series for soil C at five observation points (0.67, 1.30, 1.98, 2.30, and 2.67 m bgs) along the y-axis (Fig. 3) through the center of the model domain. Similar results were also obtained for soils A and B. Figure 5b shows the  $\theta_w$ -time series for all simulations at an observation point equivalent to the depth of the ground loop (1.98 m bgs) within the trench. For all soils, the trend of the  $\theta_w$ -time series closely followed the increase and decrease of precipitation as well as rise and fall of the GWT (Fig. 4), suggesting that the amount of precipitation and location of GWT have a significant influence on in situ moisture conditions. The initial  $\theta_w$  as well as ensuing  $\theta_w$  from capillary effects were dictated by the soil SWCCs (Fig. 1b). For all simulations, the lowest observed  $\theta_w$  (i.e., driest condition) was the residual water content of the soil.

### 6.2 Thermal Conductivity Variation

Figure 6a shows the  $\lambda$ -time series at the same five observation points for soil C as in Fig. 5a. Likewise, Fig. 6b shows the  $\lambda$ -time series at the same observation point for all simulations as in Fig. 5b. Since soils A and B had the same constant  $\lambda_{soil}$  value for the conservative analysis, only one curve for both soils is



**Fig. 5** Daily  $\theta_w$  (a) at five observation points along the y-axis for simulation of soil C and (b) at 1.98 m bgs for all simulations. Curves labeled with  $\lambda$  represent simulations modeled with constant  $\lambda_{soil}$

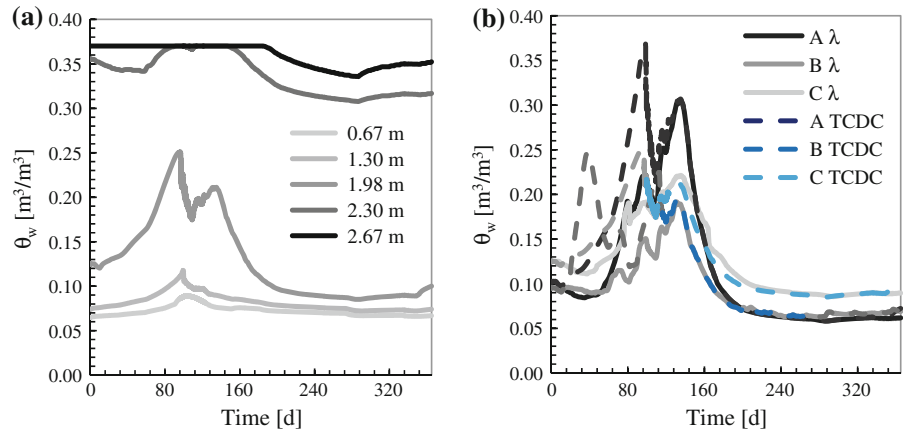
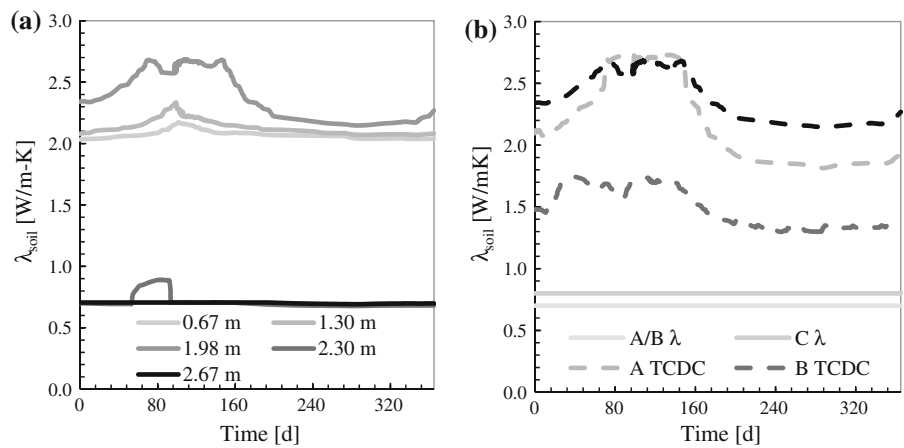


**Fig. 6** Daily  $\lambda_{soil}$  (a) at five observation points spaced along the y-axis for simulation of soil C and (b) at 1.98 m bgs for all simulations. Curves labeled with  $\lambda$  represent simulations modeled with constant  $\lambda_{soil}$

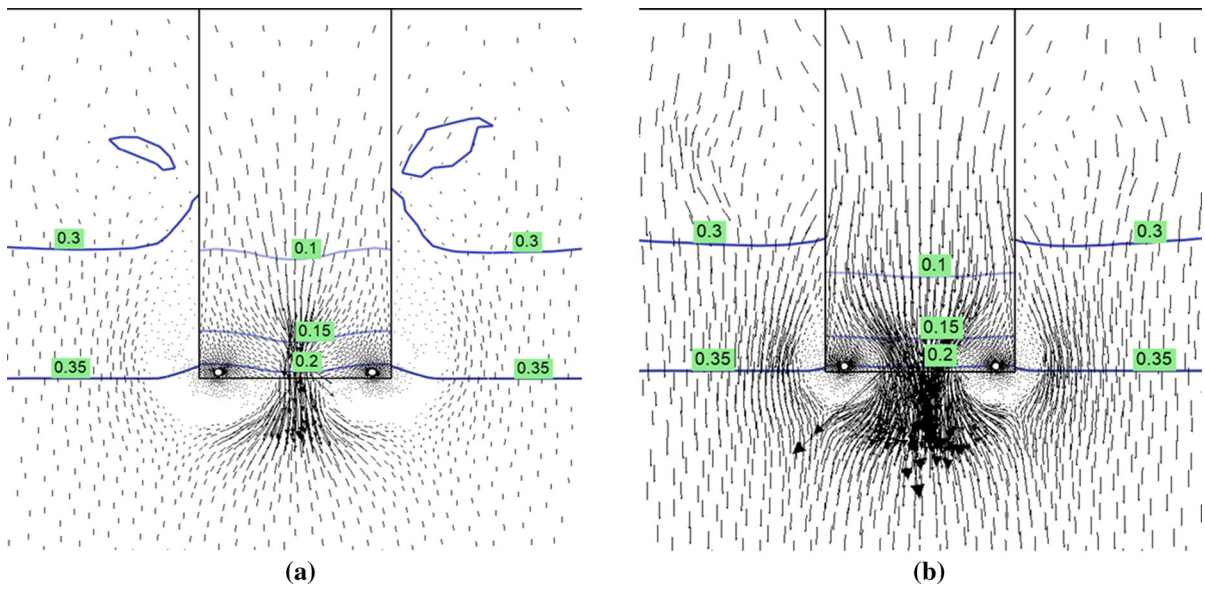


shown in Fig. 6b. As dictated by the soil TCDCs (Fig. 1a), the spatial and temporal variation of  $\lambda_{soil}$  followed the same trends as  $\theta_w$ . Even though the 2.30 m and 2.67 m bgs observation points were closer to the GWT, the  $\lambda_{soil}$  of the sandy loam was inherently lower than the  $\lambda_{soil}$  from the TCDCs of the backfill at high saturation. The backfill closest to the ground loops was able to maintain relatively high  $\lambda_{soil}$  due to precipitation infiltration and capillary rise effects from the GWT. As a consequence, the conservative and constant  $\lambda_{soil}$  values were about half to a third of the  $\lambda_{soil}$  values predicted in the simulations using the soil’s measured TCDC.

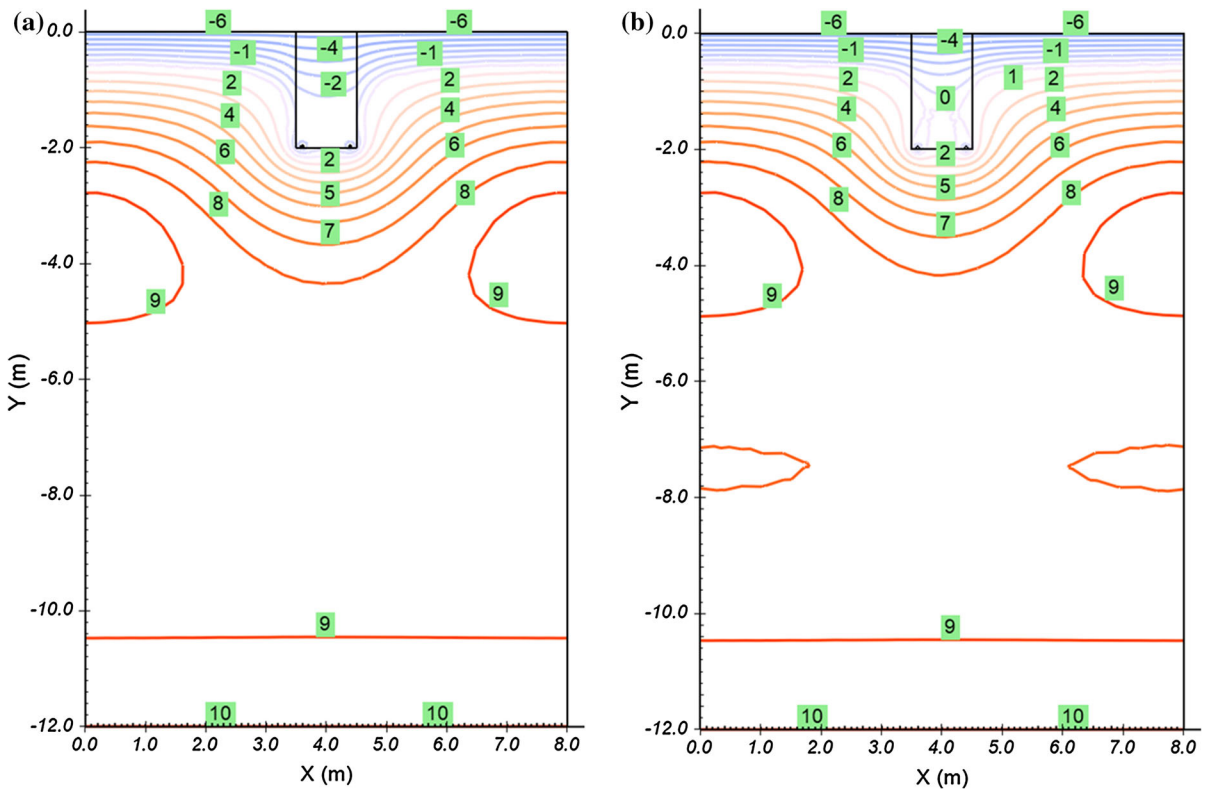
### 6.3 Water Flux Variation

Figure 7 shows  $\theta_w$  contour plots overlain with average water flux vectors for soil C at 120 days, towards the end of the first heating mode. Similar results were also

obtained for soils A and B. The size of the vectors indicates the magnitude of water flux (i.e., larger arrow indicates greater water flux). The magnitude of water flux was less in models simulated with TCDCs (Fig. 7a) and greater in models simulated with a constant  $\lambda_{soil}$  (Fig. 7b). The circular zones delineated by the water flux vectors around the ground loops suggest that water was not moving towards the ground loops but rather around the ground loops. Moreover, these circular zones suggest development of dry zone conditions since the  $\theta_w$  contours show lower  $\theta_w$  near the ground loops compared to adjacent soil outside the trench. Under continuous operation of the ground loop without resupply from moisture migration, excessive thermally induced moisture migration moving water away from the ground loops can continue to develop the dry zone. Drying conditions developed faster in models simulated with a constant  $\lambda_{soil}$  since the constant values of  $\lambda_{soil}$  were less than half of the  $\lambda_{soil}$



**Fig. 7** Water content contour profiles with moisture flux vectors after 120 days of simulation for soil C: **a** simulation modeled with TCDC and **b** simulation modeled with constant  $\lambda_{soil}$ . Contour labels are in  $\theta_w$



**Fig. 8** Ground temperature contour profiles after 365 days of simulation for soil C: **a** simulation modeled with TCDC and **b** simulation modeled with constant  $\lambda_{soil}$ . Contour labels are in  $^{\circ}C$

**Table 3** Fixed input parameters used to approximate length of ground loop in the heating mode

Parameter	Value	Dimension
Heat pump capacity	10.55	kW
Heat pump COP	4	–
EWT	–1.11	°C
$m_w$	0.584	kg/s
$\lambda_w$	0.453	W/mK
Re (turbulent flow check)	4,767	–
$D_o$	0.048	m
$\lambda_{pipe}$	0.48	W/mK
Avg. $T_g$ at ground surface	7.7	°C

**Table 4** Values of  $\lambda_{soil}$  from simulation results used to approximate length of ground loop

Soil (TCDC or $\lambda$ ) →	A ( $\lambda$ )	A (TCDC)	B ( $\lambda$ )	B (TCDC)	C ( $\lambda$ )	C (TCDC)
$\lambda_{soil}$ (W/mK)	0.7	1.8	0.7	1.3	0.8	2.1

predicted by using the TCDCs (Fig. 5b). As illustrated in comparing Fig. 7a, b, the  $\theta_w$  contours show greater water retention in the trench for the simulation modeled with the TCDC compared to the simulation modeled with constant  $\lambda_{soil}$ .

### 6.4 Ground Temperature Variation

Figure 8 shows ground temperature contour plots for soil C at the end of 365 days when the simulation finished in the heating mode. Similar results were also obtained for soils A and B. In models simulated with TCDCs, the temperature contours were farther apart and the overall temperature profile was more widespread (e.g., 8 °C temperature contour extends lower in Fig. 8a than b), which was expected since heat transfer between the ground and ground loop is more effective at higher  $\lambda_{soil}$ . In general, temperature contours in the trench also showed that the ground temperature closest to the ground loop was colder (and were also hotter in the cooling mode) in simulations modeled using a TCDC compared to simulations modeled using constant  $\lambda_{soil}$ . At the end of 1 year of operation, the greatest difference between ground temperature contours obtained from models simulated with a TCDC versus a constant  $\lambda_{soil}$  was about 0.2 m.

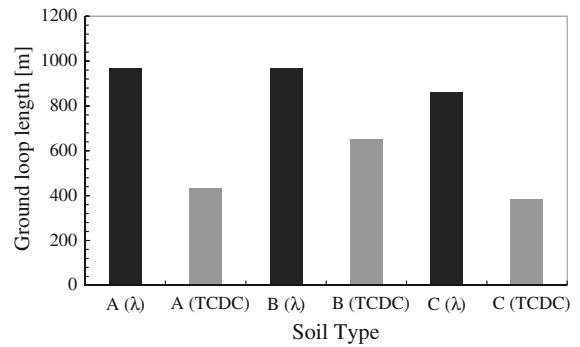


**Fig. 9** Approximate length of ground loop for each simulated soil

Stable temperature contours near the bottom of the domain indicate the lower boundary temperature did have not a significant effect during the simulations.

### 6.5 Length of Ground Loop

Approximate lengths of ground loop for the specified GSHP system were calculated using the input data in Table 3 and Eq. (14) for each simulation. To approximate the longest required length of ground loop, the lowest observed value of  $\lambda_{soil}$  during each simulation was used (Table 4). Figure 9 presents the total length of ground loop required for each soil and indicates that the difference in  $\lambda_{soil}$  had a significant effect. The length of the ground loop was 25–50 % longer for every soil simulated with constant  $\lambda_{soil}$  rather than its TCDC. These simulation results demonstrate the importance of accurately modeling temporal and spatial moisture profiles to predict the thermal behavior of backfill surrounding horizontal ground loops.

## 7 Conclusion

Coupled TCDCs and SWCCs were used in horizontal ground loop modeling to predict the moisture-dependent behavior of  $\lambda_{soil}$ . By using the soil’s SWCC and TCDC,  $\lambda_{soil}$  was more accurately predicted by incorporating the effects of moisture migration. The SWCC provided determination of soil moisture variability in response to transient hydraulic and thermal gradients from climatic variations and ground loop operation. Furthermore, by coupling the TCDC, the thermal response of the surrounding soil and  $\lambda_{soil}$  were

determined. In the performed simulation scenarios, values of  $\lambda_{\text{soil}}$  predicted from the soil's TCDC were nearly twice the conservative and constant  $\lambda_{\text{soil}}$ . As a consequence, using the soil's TCDC rather than a conservative and constant value of  $\lambda_{\text{soil}}$  also resulted in 25–50 % shorter loops.

In extremely arid or wet climates, where soil moisture is not expected to vary over a wide range, the current state of practice of selecting a constant  $\lambda_{\text{soil}}$  representative of the dry or saturated condition may serve as a suitable design parameter for designing shallow horizontal GSHP systems. However, in regions where the soil is susceptible to moisture migration, the SWCC and TCDC of the backfill and native soil are useful to model actual conditions. These finite-element simulations showed that coupled SWCC and TCDC models are capable of capturing coupled heat and moisture flow in shallow horizontal ground loop applications and have potential value in improving the design of the ground loop. Performing these simulations for the design life of the GSHP system and using nonisothermal boundary conditions should be considered in the future for a more complete approach. Furthermore, the implementation of experimental testing (i.e., installing and monitoring temperature and moisture sensors at a shallow horizontal ground loop site) would provide validation and verification of the simulated models.

**Acknowledgments** Mr. Jim Zhang and Mr. Rob Thode of SoilVision® Systems are gratefully acknowledged for their assistance in the numerical simulations. Special thanks are also offered to Mr. Jun Yao and Mr. Hyunjun Oh of the University of Wisconsin-Madison for their efforts in conducting laboratory experiments.

## References

- Abu-Hamdeh NH, Reeder RC (2000) Soil thermal conductivity effects of density, moisture, salt concentration, and organic matter. *Soil Sci Soc Am J* 64(4):1285–1290
- Agus SS, Schanz T (2005) Comparison of four methods for measuring total suction. *Vadose Zone J* 4(4):1087–1095
- ASHRAE (2007) Geothermal energy. ASHRAE handbook: HVAC applications, American society of heating, refrigerating and air conditioning engineers
- Benazza A, Blanco E, Aichouba M, Rio JL, Laouedj S (2011) Numerical investigation of horizontal ground coupled heat exchanger. *Energy Procedia* 6:29–35
- Campbell GS, Jungbauer JD Jr, Bidlake WR, Hungerford RD (1994) Predicting the effect of temperature on soil thermal conductivity. *Soil Sci* 158(5):307–313
- Chiasson AD (2010) Modeling horizontal ground heat exchangers in geothermal heat pump systems. In: Proceedings of COMSOL conference
- Chong CSA, Gan G, Verhoef A, Garcia RG, Vidale PL (2012) Simulation of thermal performance of horizontal slinky-loop heat exchangers for ground source heat pumps. *Appl Energy* 104:603–610
- Congedo PM, Colangelo G, Starace G (2012) CFD simulations of horizontal ground heat exchangers: a comparison among different configurations. *Appl Therm Eng* 33:24–32
- Côté J, Konrad JM (2005) A generalized thermal conductivity model for soils and construction materials. *Can Geotech J* 42(2):443–458
- Demir H, Koyun A, Temir G (2009) Heat transfer of horizontal parallel pipe ground heat exchanger and experimental verification. *Appl Therm Eng* 29(2):224–233
- Farouki OT (1981) Thermal properties of soils. United States Army Corps of Engineers CRREL, Hanover
- Florides G, Kalogirou S (2007) Ground heat exchangers—a review of systems, models and applications. *Renew Energy* 32(15):2461–2478
- Fredlund DG, Xing A (1994) Equations for the soil–water characteristic curve. *Can Geotech J* 31(4):521–532
- Hillel D (1982) Introduction to soil physics. Academic Press, New York
- İnalı M, Esen H (2005) Seasonal cooling performance of a ground-coupled heat pump system in a hot and arid climate. *Renew Energy* 30(9):1411–1424
- Incropera FP, DeWitt DP, Bergman TL, Lavine AS (2006) Fundamentals of heat and mass transfer, 6th edn. Wiley, Hoboken
- Krishnapillai SH, Ravichandran N (2012) New soil–water characteristic curve and its performance in the finite-element simulation of unsaturated soils. *Int J Geomech* 12(3):209–219
- Kusuda T, Achenbach PR (1965) Earth temperature and thermal diffusivity at selected stations in the United States. National Bureau of Standards
- Leij FJ, Alves WJ, van Genuchten MT, Williams JR (1996) The UNSODA unsaturated hydraulic database. U.S. Environmental Protection Agency, Cincinnati, Ohio
- Likos WJ, Olson HS, Jaafar R (2012) Comparison of laboratory methods for measuring thermal conductivity of unsaturated soils. *GeoCongress 2012 state of the art and practice in geotechnical engineering*, ASCE: 4366–4375
- Neher JH, McGrath MH (1957) The calculation of the temperature rise and load capability of cable systems. *AIEE Trans* 76(3):752–772
- Remund C, Carda R (2009) Ground source heat pump residential and light commercial design and installation guide. Oklahoma State University and International Ground Source Heat Pump Association
- Salomone LA, Kovacs WD (1984) Thermal resistivity of soils. *J Geotech Eng* 110(3):375–389
- Smits KM, Sakaki T, Limsuwat A, Illangasekare TH (2010) Thermal conductivity of sands under varying moisture and porosity in drainage–wetting cycles. *Vadose Zone J* 9(1):172–180
- Smits KM, Sakaki T, Howington SE, Peters JF, Illangasekare TH (2012) Temperature dependence of thermal properties of sands across a wide range of temperatures (30–70 °C). *Vadose Zone J* 12(1):1–8

- Tarnawski VR, Leong WH, Momose T, Hamada Y (2009) Analysis of ground source heat pumps with horizontal ground heat exchangers for northern Japan. *Renew Energy* 34(1):127–134
- Thode R, Zhang J (2009) SVHeat 1D/2D/3D geothermal modeling software theory manual. SoilVision® Systems Ltd
- van Genuchten MT (1980) A closed-form equation for predicting the hydraulic conductivity of unsaturated soils. *Soil Sci Soc Am J* 44(5):892–898
- Williams GP, Gold LW (1976) Ground temperatures. *Can Build Dig*. National Research Council of Canada, Institute for Research in Construction
- Woodward NR, Tinjum JM, Wu R (2013) Water migration impacts on thermal resistivity testing procedures. *Geotech Test J* 36(6):948–955
- Wu Y, Gan G, Verhoef A, Vidale PL, Gonzalez RG (2010) Experimental measurement and numerical simulation of horizontal-coupled slinky ground source heat exchangers. *Appl Therm Eng* 30(16):2574–2583